

# Supplement to “A global dataset of $\delta^{13}\text{C}$ - $\text{CH}_4$ source signatures and associated uncertainties (1998–2022), with a sensitivity analysis to support isotopic inversions” by Emeline Tapin *et al.*

## S1 Additional methods

### S1.1 Stable carbon isotope reference scale

All  $\delta^{13}\text{C}$ - $\text{CH}_4$  values reported in this study are expressed relative to the Vienna Pee Dee Belemnite (VPDB) standard, the internationally accepted reference for stable carbon isotope ratios. Historically, earlier atmospheric  $\delta^{13}\text{C}$ - $\text{CH}_4$  simulations used the Pee Dee Belemnite (PDB) reference scale defined by Craig (1957), where  $R_{\text{PDB}} = 1.12372 \times 10^{-2}$  is the standard  $^{13}\text{C}/^{12}\text{C}$  ratio. The current VPDB scale adopts a slightly different value,  $R_{\text{VPDB}} = 0.011113 \pm 0.000022$  (95% confidence level; Camin et al. 2025).

To assess the consistency between these reference scales, we repeated our model calculations using the updated VPDB standard. The resulting differences in  $\delta^{13}\text{C}$ - $\text{CH}_4$  outputs were negligible, with a mean offset of less than  $-6\text{e-}5\%$  over the 24-year simulation period. This confirms that the choice of reference standard does not materially affect the results presented in this work.

### S1.2 Method for aggregating isotopic signatures from sub-sectors into sectors

The aggregation of isotopic signatures from sub-sectors into sectoral values was performed using a mass-weighted approach based on the underlying carbon isotopic ratios. When fluxes are provided in mass units rather than moles, appropriate molar mass ratios are applied to ensure consistency. The procedure is as follows:

For each sub-sector  $i$ :

1. The isotopic signature  $\delta^{13}\text{C}_i$  is first converted to the corresponding isotopic ratio  $R_i$  relative to the VPDB standard:

$$R_i = \left(1 + \frac{\delta^{13}\text{C}_i}{1000}\right) R_{\text{PDB}},$$

where  $R_{\text{PDB}}$  is the reference  $^{13}\text{C}/^{12}\text{C}$  ratio of the Pee Dee Belemnite (PDB) standard.

2. The partial fluxes of  $^{12}\text{CH}_4$  and  $^{13}\text{CH}_4$  for each sub-sector are then calculated as:

$$F_{12,i} = \frac{F_{\text{total},i} M_{12\text{C}}/M_{\text{CH}_4}}{1 + R_i} \quad F_{13,i} = \frac{F_{\text{total},i} R_i M_{13\text{C}}/M_{\text{CH}_4}}{1 + R_i},$$

where  $F_{\text{total},i}$  is the total methane flux for subcategory  $i$  (in mass units), and  $M_{12\text{C}}$ ,  $M_{13\text{C}}$  and  $M_{\text{CH}_4}$  are the molar masses of  $^{12}\text{C}$ ,  $^{13}\text{C}$  and  $\text{CH}_4$ , respectively.

3. The fluxes are then summed over all subcategories within a given sector  $s$ :

$$25 \quad F_{12}^s = \sum_i F_{12,i}, \quad F_{13}^s = \sum_i F_{13,i}.$$

4. The aggregated isotopic ratio for the sector is calculated as:

$$R^s = \frac{F_{13}^s}{F_{12}^s}.$$

5. Finally, the aggregated isotopic signature for the sector is computed as:

$$\delta^{13}\text{C}^s = \left[ \frac{R^s}{R_{\text{PDB}}} \frac{M_{12\text{C}}}{M_{13\text{C}}} - 1 \right] \times 1000.$$

30 This approach ensures that the aggregated isotopic signature is correctly weighted by the contribution of each subsector to the total flux of the sector.

## S2 Supplementary tables

### S2.1 List of acronyms and datasets used in this study

**Table S1.** List of acronyms used in this study.

<b>Acronym</b>	<b>Definition / Source</b>
CIF	Community Inversion Framework
VPDB	Vienna Pee Dee Belemnite (standard for stable carbon isotope ratios)
KIE	Kinetic Isotope Effect
FFG	Fossil Fuel exploitation and Geological sources
AGW	Agriculture and Waste
BB	Biomass and Biofuel Burning
WET	Wetlands
NAT	Other Natural Sources
EDGARv8	Emissions Database for Global Atmospheric Research (Crippa et al., 2023)
GFED4s	Global Fire Emissions Database (van Wees et al., 2022)
GMB	Global Methane Budget (Martinez et al., 2024; Saunio et al., 2025)
EMID	European Methane Isotope Database (Menoud et al., 2024)
GFEIv2	Global Fuel Exploitation Inventory (Scarpelli et al., 2022)
CEDSv2021	Community Emissions Data System (O'Rourke et al., 2021)
GAINsv4	Greenhouse Gas and Air Pollution Interactions and Synergies model (Höglund-Isaksson et al., 2020)
RSD	Relative Standard Deviation
SD	Standard Deviation

## S2.2 European fossil-fuels isotopic signature aggregation

**Table S2.** Country-level weighted mean  $\delta^{13}\text{C-CH}_4$  values (‰) for oil & gas and coal emissions in Europe, derived from data compiled by Lan et al. (2021) and Menoud et al. (2022).  $N$  indicates the number of individual measurements contributing to each dataset. A weighted mean is calculated when data from both sources are available.

Country	$\delta^{13}\text{C-CH}_4$ (Lan et al., 2021) (‰) / $N$	$\delta^{13}\text{C-CH}_4$ (Menoud et al., 2022) (‰) / $N$	Weighted mean (‰)
<b>Oil &amp; Gas</b>			
France	-44.0 / 28	-44.8 / 30	-44.4
United Kingdom	-39.2 / 13	-40.2 / 135	-40.1
Germany	-43.8 / 176	-39.3 / 29	-43.2
Poland	-47.0 / 57	-44.9 / 27	-46.3
Romania	-48.3 / –	-37.7 / 143	-37.7
Netherlands	–	-44.8 / 11	-44.8
<b>Coal</b>			
United Kingdom	-40.1 / 23	-48.8 / 4	-41.2
Germany	-43.1 / 90	-44.7 / 3	-43.2
Poland	-49.5 / 64	-49.2 / 64	-49.4

## 35 S2.3 Monte Carlo ensemble simulations of isotopic source signatures

**Table S3.** Parameters used for the Monte Carlo ensemble simulations of isotopic source signatures. For each of the five main source sectors, normal distributions were defined based on literature-derived mean and standard deviation values (see Section 4.1.3). Five ensemble members were drawn per sector to represent the uncertainty in  $\delta^{13}\text{CH}_4$  source signatures. The table includes sector-specific mean isotopic signatures and their variability, with spatial granularity used for Monte Carlo: 110 countries (Natural Earth dataset, free vector and raster map data at [naturalearthdata.com](http://naturalearthdata.com)) for anthropogenic sectors (FFG, AGW) reflecting country-level variability, and 18 GCP regions (Saunois et al., 2020) for natural sectors (BB, WET, NAT) reflecting coarser regional variability.

Sector	Mean signature [‰]	Standard deviation ( $1\sigma$ ) [%]	Spatial granularity
Fossil Fuel & Geological (FFG)	-44.2	13.9	110 countries
Agriculture and Waste (AGW)	-60.2	5.5	110 countries
Biomass & Biofuel Burning (BB)	-24.3	24.9	18 GCP regions
Wetlands (WET)	-58.6	12.8	18 GCP regions
Other Natural (NAT)	-51.9	10.4	18 GCP regions

### S3 Supplementary figures

#### S3.1 Detailed sub-sectors $\delta^{13}\text{C}\text{-CH}_4$ source signature maps

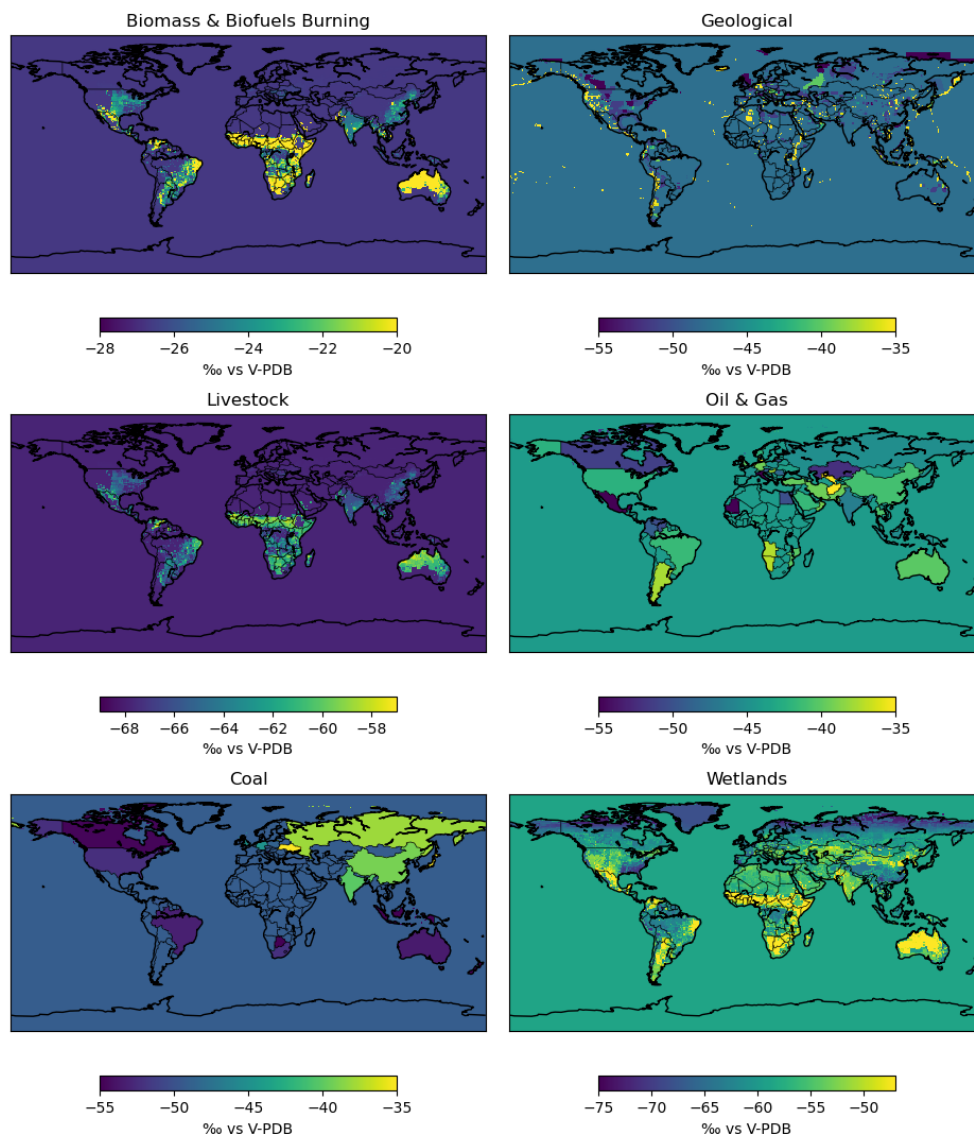


**Figure S1.** Maps of  $\delta^{13}\text{C}\text{-CH}_4$  subcategories, showing isotopic signatures by source subcategory. Sources for sector isotopic signatures are: Biomass – Biofuels Burning (Lan et al., 2021), Geological (Etiopie et al., 2019), Livestock (Lan et al., 2021), Oil and Gas (Lan et al., 2021; Menoud et al., 2022), Coal (Lan et al., 2021; Menoud et al., 2022), and Wetlands (Oh et al., 2022).

### S3.2 Detailed sub-sectors CH<sub>4</sub> emissions maps

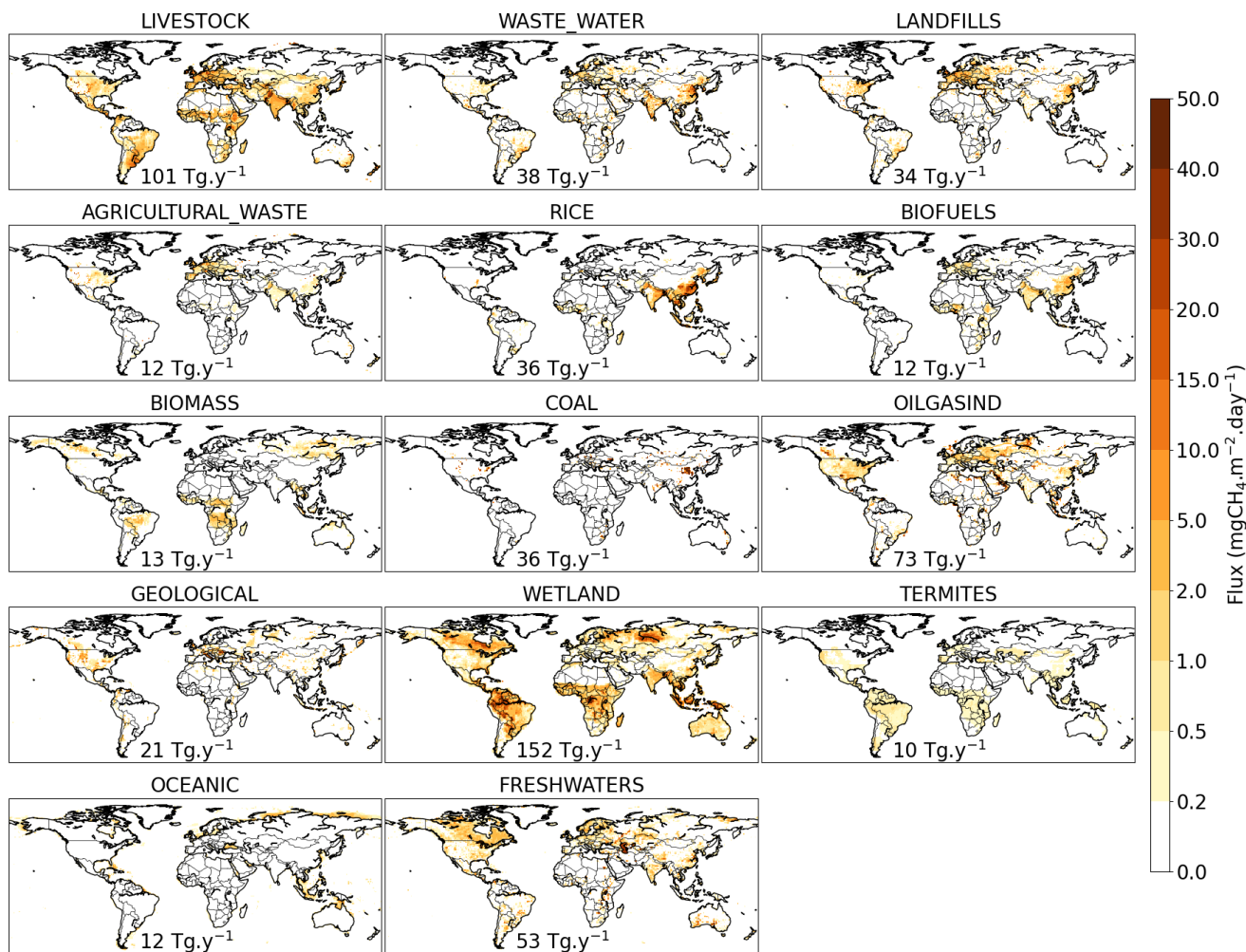


**Figure S2.** Mean methane emissions (1998–2022) for each sub-sector contributing to the five main CH<sub>4</sub> source sectors, expressed in mgCH<sub>4</sub> m<sup>-2</sup> day<sup>-1</sup>. Each panel shows the spatial distribution of the average flux over the 1998–2022 period, with the total subcategory emission (in Tg yr<sup>-1</sup>) indicated. Anthropogenic emissions (e.g., RICE, LANDFILLS, LIVESTOCK, WASTEWATER, AGRICULTURAL WASTE, BIOFUELS, COAL, OIL AND GAS) are from EDGARv8.0 (Crippa et al., 2023). Biomass burning emissions (BIOMASS) are derived from GFED4s (van Wees et al., 2022). Wetland emissions correspond to the climatological mean of 11 process-based models from the Global Methane Budget (GMB) (Martinez et al., 2024). Freshwater emissions are based on CH<sub>4</sub> flux maps from Stavert et al. (2022), with spatial rescaling following Martinez et al. (2024). Geological, termite, and oceanic emissions follow the GMB prior dataset, based respectively on Etiope et al. (2019), the S. Castaldi model for termites (Martinez et al., 2024), and oceanic emissions from Weber et al. (2019). All datasets were harmonised to a common 1° × 1° grid.

### S3.3 Sensitivity analysis

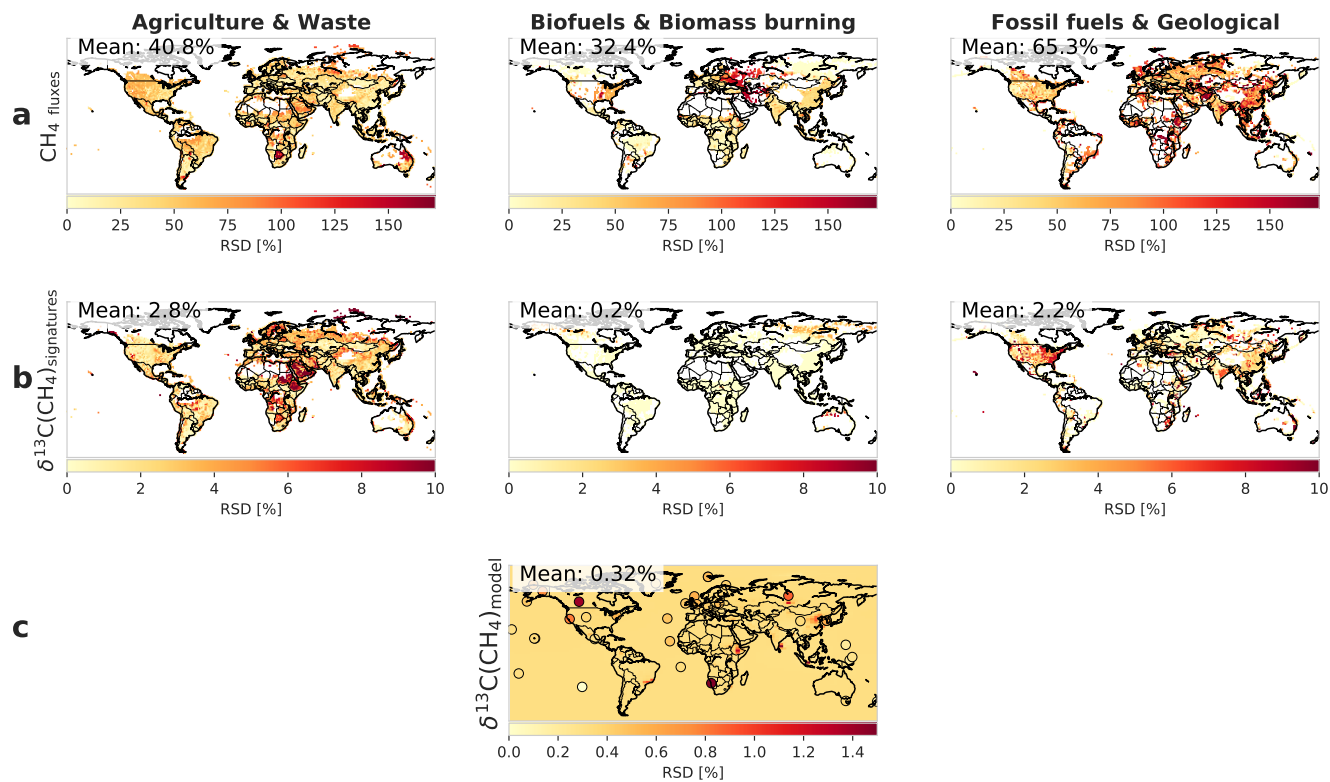


**Figure S3.** (a) RSD (in %) of the fluxes among different prior datasets (GAINSv4, CEDSv2021, GFEIv2, EDGARv8) (over 2016–2020) at surface level. Values are only displayed when the associated CH<sub>4</sub> flux is higher than  $0.2 \text{ mgCH}_4 \cdot \text{m}^{-2} \cdot \text{day}^{-1}$ , for aggregated categories. (b) RSD of the resulting  $\delta^{13}\text{C}\text{-CH}_4$  source signature by aggregated category. (c) RSD of the  $\delta^{13}\text{C}\text{-CH}_4$  signals from the forward model outputs at surface level. Coloured circles indicate RSD of observed  $\delta^{13}\text{C}\text{-CH}_4$  values at each surface station over the study period.

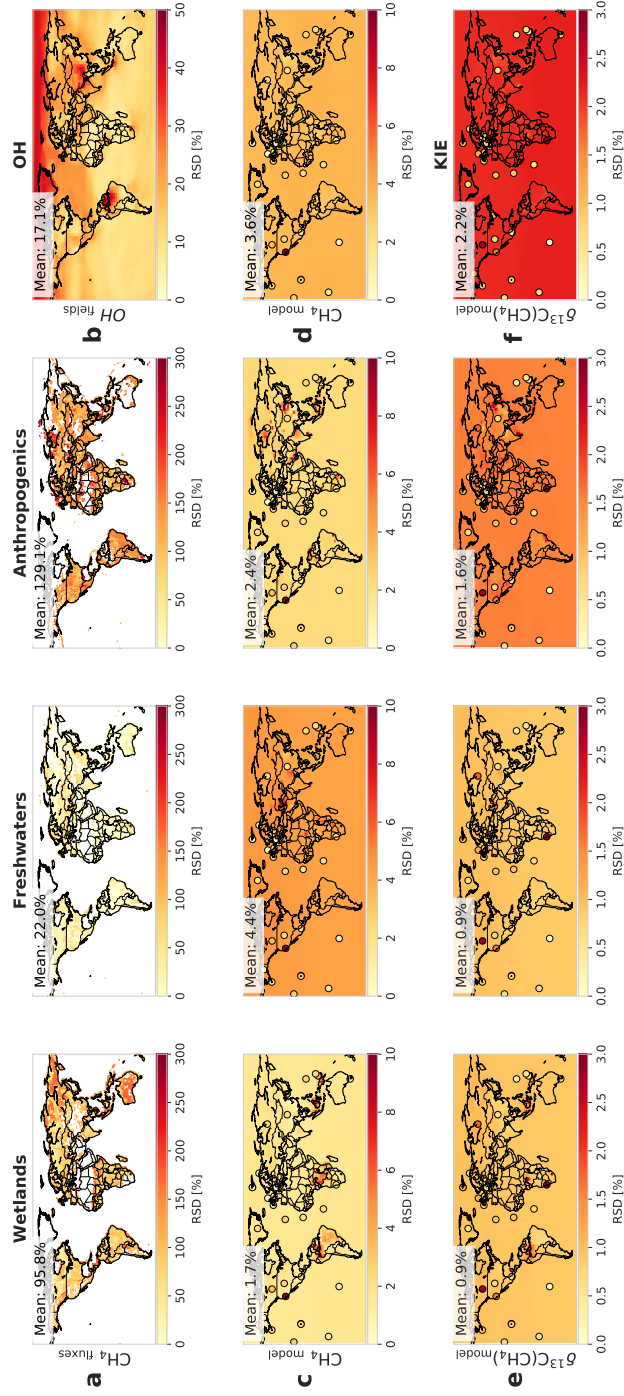


**Figure S4.** RSD (in %) over 2016–2020 at surface level. (a) RSD of CH<sub>4</sub> emissions from wetlands, freshwaters, and anthropogenic sectors (AGW, FFG, BB). Values are only displayed when the associated CH<sub>4</sub> flux exceeds 0.2 mg CH<sub>4</sub>·m<sup>-2</sup>·day<sup>-1</sup>. (b) RSD of the total tropospheric OH column (pressure levels below 250 hPa). (c) RSD of CH<sub>4</sub> mole fractions at surface level from forward model outputs, driven by uncertainty in emission fluxes. Coloured circles indicate RSD of observed CH<sub>4</sub> mole fractions at surface stations with co-located  $\delta^{13}\text{C}(\text{CH}_4)$  measurements. (d) Same as (c), but driven by uncertainty in OH fields. (e) RSD of  $\delta^{13}\text{C}-\text{CH}_4$  values at surface level from forward model outputs, driven by uncertainty in emission fluxes. Coloured circles indicate RSD of observed  $\delta^{13}\text{C}-\text{CH}_4$  values at the same stations. (f) Same as (e), but driven by uncertainty in kinetic isotope effects (KIE) during CH<sub>4</sub> oxidation.

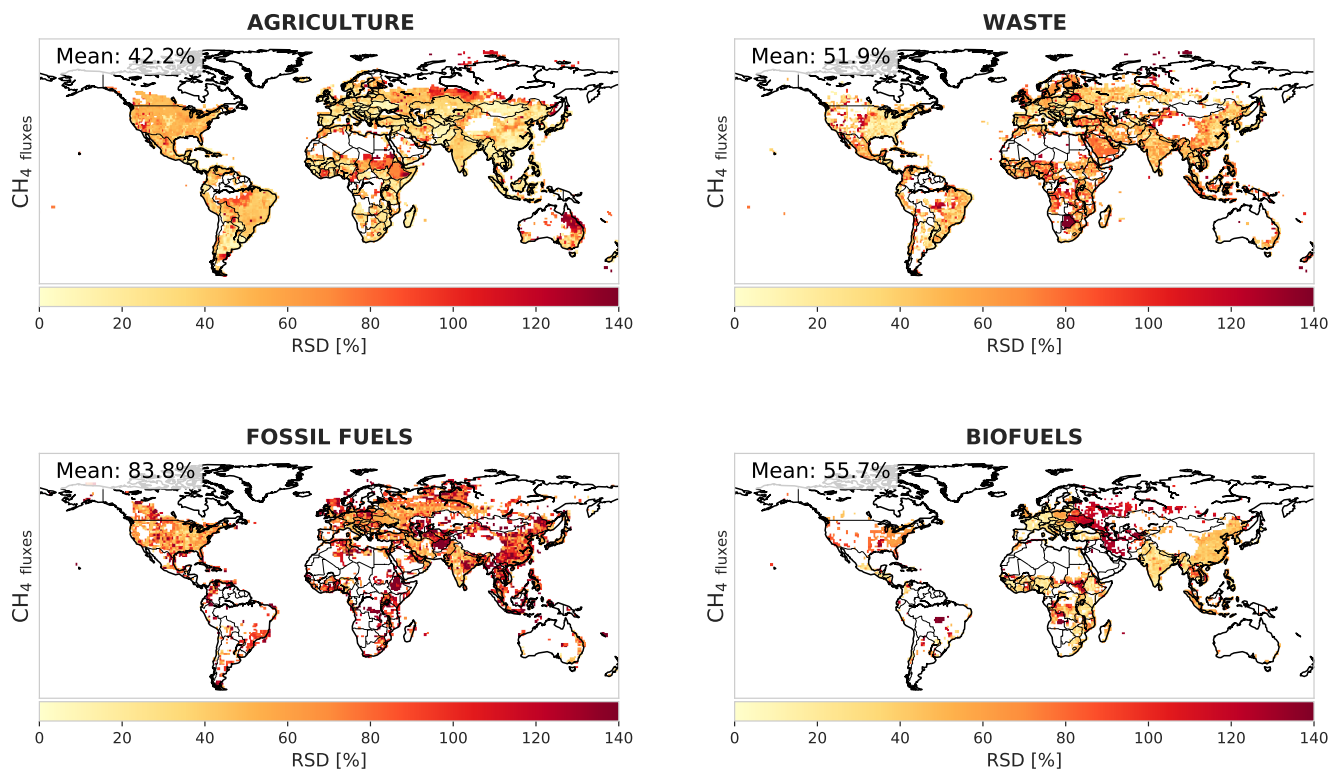


**Figure S5.** RSD (in %) of fluxes included in anthropogenics sector of annual mean CH<sub>4</sub> fluxes across four inventories (EDGARv8, CEDS, GAINS, GFEI) over (over 2016–2020), shown by emission sub-sector. Values are only displayed when the associated CH<sub>4</sub> flux is higher than  $0.2 \text{ mgCH}_4 \cdot \text{m}^{-2} \cdot \text{day}^{-1}$

**Sub-sector grouping used in this figure:**

*AGRICULTURE:* LIVESTOCK, RICE

*WASTE:* AGRICULTURAL\_WASTE, LANDFILLS, WASTE\_WATER

*FOSSIL FUELS:* COAL, OILGASIND

*BIOFUELS:* BIOFUELS

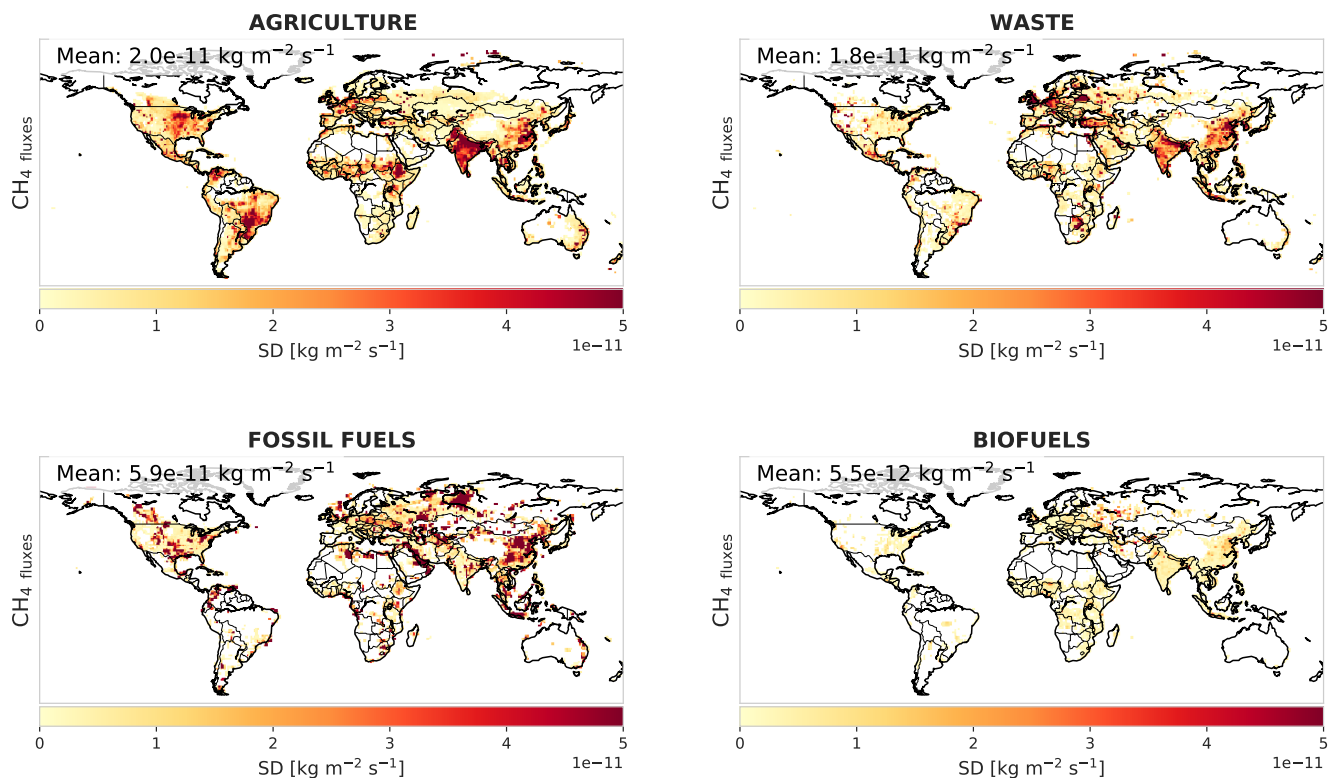


**Figure S6.** SD (in  $\text{kg} \cdot \text{m}^{-2} \cdot \text{s}^{-1}$ ) of fluxes included in the anthropogenic sector of annual mean CH<sub>4</sub> fluxes across four inventories (EDGARv8, CEDS, GAINS, GFEI) over 2016–2020, shown by emission sub-sector. Values are only displayed when the associated CH<sub>4</sub> flux is higher than  $0.2 \text{ mgCH}_4 \cdot \text{m}^{-2} \cdot \text{day}^{-1}$ .

**Sub-sector grouping used in this figure:**

*AGRICULTURE:* LIVESTOCK, RICE

*WASTE:* AGRICULTURAL\_WASTE, LANDFILLS, WASTE\_WATER

*FOSSIL FUELS:* COAL, OILGASIND

*BIOFUELS:* BIOFUELS

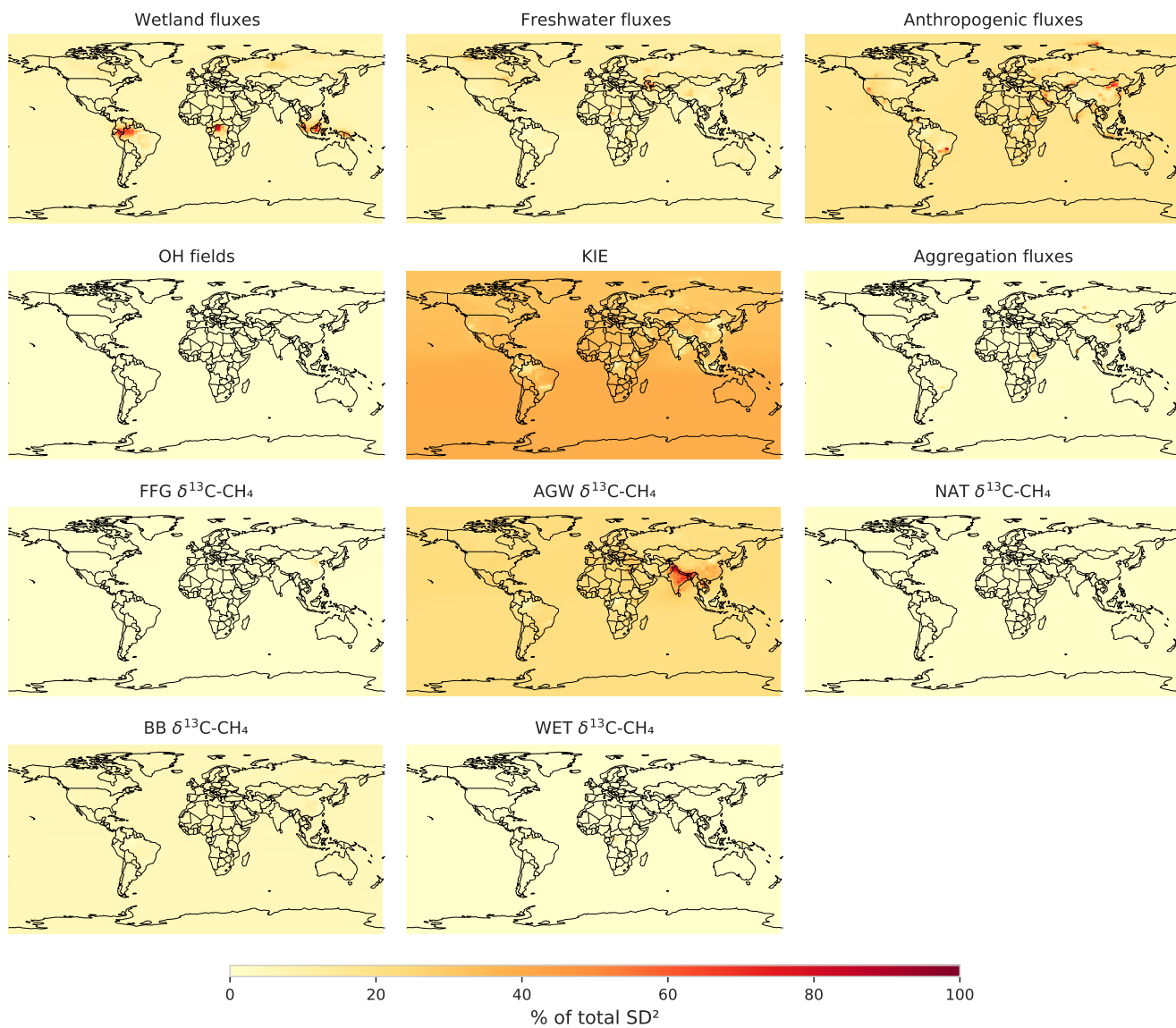


**Figure S8.** Relative contribution (in %) of each parameter to the total variance of simulated atmospheric  $\delta^{13}\text{C-CH}_4$  at each model grid cell. Each panel represents one sensitivity parameter tested. Colors indicate the percentage contribution of the squared standard deviation of each parameter to the total variance across all parameters. Values are calculated independently at each grid cell.

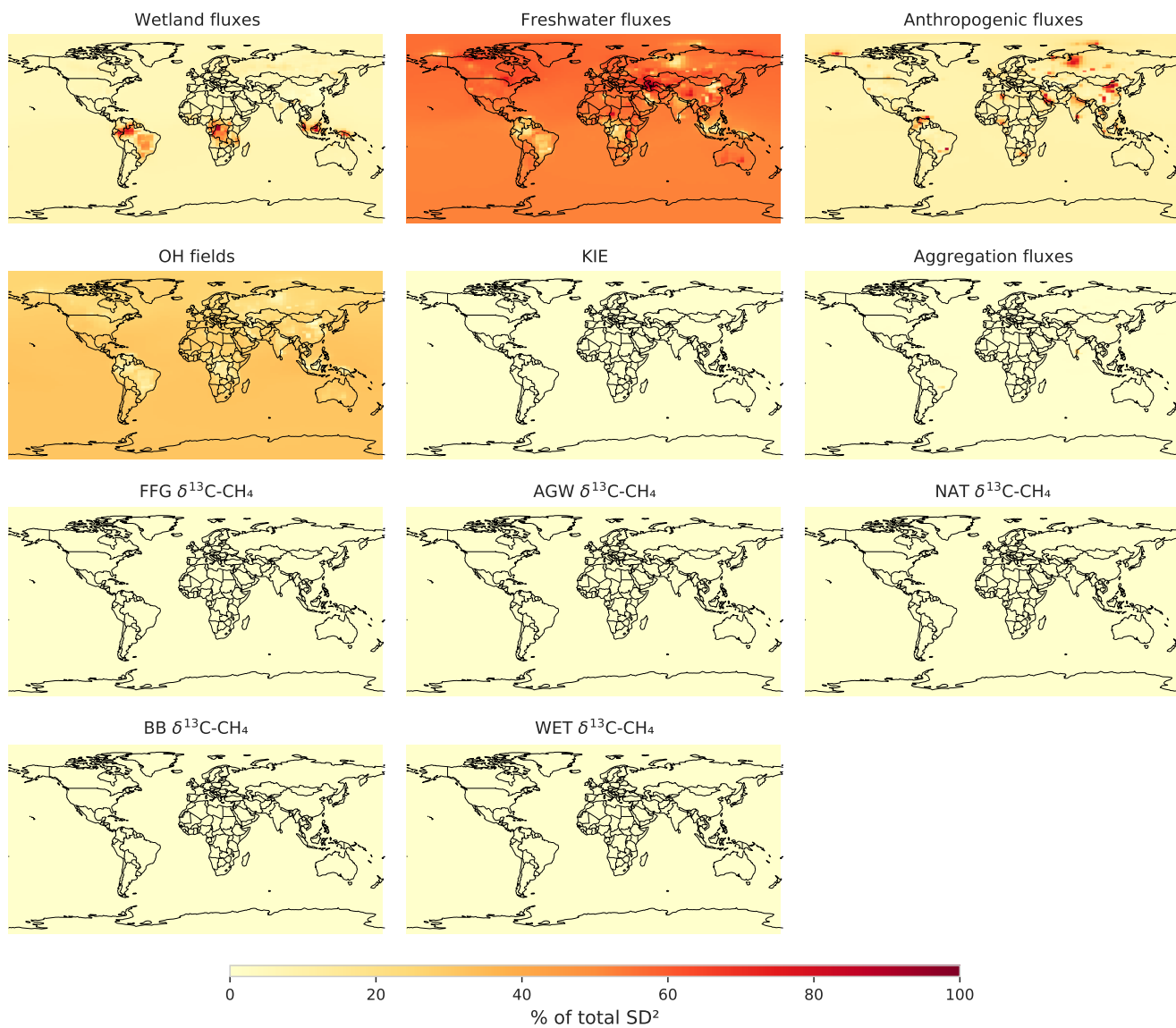


**Figure S9.** Relative contribution (in %) of each parameter to the total variance of simulated atmospheric  $\text{CH}_4$  at each model grid cell. Each panel represents one sensitivity parameter tested. Colors indicate the percentage contribution of the squared standard deviation of each parameter to the total variance across all parameters. Values are calculated independently at each grid cell.

## 40 References

- Camin, F., Besic, D., Brewer, P. J., Allison, C. E., Coplen, T. B., Dunn, P. J. H., Gehre, M., Gröning, M., Meijer, H. A. J., Hélie, J.-F., Iacumin, P., Kraft, R., Krajnc, B., Kümmel, S., Lee, S., Meija, J., Mester, Z., Mohn, J., Moossen, H., Qi, H., Skrzypek, G., Sperlich, P., Viallon, J., Wassenaar, L. I., and Wielgosz, R. I.: Stable Isotope Reference Materials and Scale Definitions—Outcomes of the 2024 IAEA Experts Meeting, *Rapid Communications in Mass Spectrometry*, 39, e10018, <https://doi.org/10.1002/rcm.10018>, 2025.
- 45 Craig, H.: Isotopic Standards for Carbon and Oxygen and Correction Factors for Mass-Spectrometric Analysis of Carbon Dioxide, *Geochimica et Cosmochimica Acta*, 12, 133–149, [https://doi.org/10.1016/0016-7037\(57\)90024-8](https://doi.org/10.1016/0016-7037(57)90024-8), 1957.
- Crippa, M., Guizzardi, D., Schaaf, E., Monforti-Ferrario, F., Quadrelli, R., Risquez Martin, A., Rossi, S., Vignati, E., Muntean, M., Brandao De Melo, J., Oom, D., Pagani, F., Banja, M., Taghavi-Moharamli, P., Köykkä, J., Grassi, G., Branco, A., and San-Miguel, J.: GHG Emissions of All World Countries: 2023, Publications Office of the European Union, ISBN 978-92-68-07550-0, 2023.
- 50 Etiope, G., Ciotoli, G., Schwietzke, S., and Schoell, M.: Gridded Maps of Geological Methane Emissions and Their Isotopic Signature, *Earth System Science Data*, 11, 1–22, <https://doi.org/10.5194/essd-11-1-2019>, 2019.
- Höglund-Isaksson, L., Gómez-Sanabria, A., Klimont, Z., Rafaj, P., and Schöpp, W.: Technical Potentials and Costs for Reducing Global Anthropogenic Methane Emissions in the 2050 Timeframe –Results from the GAINS Model, *Environmental Research Communications*, 2, 025 004, <https://doi.org/10.1088/2515-7620/ab7457>, 2020.
- 55 Lan, X., Basu, S., Schwietzke, S., Bruhwiler, L. M. P., Dlugokencky, E. J., Michel, S. E., Sherwood, O. A., Tans, P. P., Thoning, K., Etiope, G., Zhuang, Q., Liu, L., Oh, Y., Miller, J. B., Pétron, G., Vaughn, B. H., and Crippa, M.: Improved Constraints on Global Methane Emissions and Sinks Using  $\delta^{13}\text{C}\text{-CH}_4$ , *Global Biogeochemical Cycles*, 35, e2021GB007 000, <https://doi.org/10.1029/2021GB007000>, 2021.
- Martinez, A., Saunio, M., Poulter, B., Bousquet, P., Canadell, J. G., Jackson, R. B., Dlugokencky, E. J., Ciais, P., Bastviken, D., Blake, D. R., Castaldi, S., Etiope, G., Gedney, N., Höglund-Isaksson, L., Hugelius, G., Ito, A., Kleinen, T., Krummel, P. B., Liu, L., McDonald, K. C., Melton, J. R., Müller, J., Murguia-Flores, F., Niwa, Y., Noce, S., Parker, R. J., Peng, C., Ramonet, M., Riley, W. J., Rosentretter, J. A., Segers, A., Smith, S. J., Tian, H., Tubiello, F. N., Tsuruta, A., Weber, T. S., van der Werf, G. R., Worthy, D., Yoshida, Y., Zhang, W., Zhang, Z., Zheng, B., Zhu, Q., Zhu, Q., and Zhuang, Q.: Supplemental Data of the Global Carbon Project Methane Budget 2024 V1, <https://doi.org/10.18160/GKQ9-2RHT>, 2024.
- 60 Menoud, M., van der Veen, C., Lowry, D., Fernandez, J. M., Bakkaloglu, S., France, J. L., Fisher, R. E., Maazallahi, H., Stanisavljević, M., Nečki, J., Vinkovic, K., Łakomiec, P., Rinne, J., Korbeň, P., Schmidt, M., Defratyka, S., Yver-Kwok, C., Andersen, T., Chen, H., and Röckmann, T.: New Contributions of Measurements in Europe to the Global Inventory of the Stable Isotopic Composition of Methane, *Earth System Science Data*, 14, 4365–4386, <https://doi.org/10.5194/essd-14-4365-2022>, 2022.
- Menoud, M., Thomas, R., Carina, v. d. V., Julianne, F., Semra, B., Dave, L., James, F., Rebecca, F., Hossein, M., Piotr, K., Martina, S., Mila, S., Jaroslaw, N., Patryk, Ł., Janne, R., Sara, D., Camille, Y.-K., Katarina, V., Truls, A., and Huilin, C.: The European Methane
- 70 Isotope Database Coupled with a Global Inventory of Fossil and Non-Fossil  $\delta^{13}\text{C}\text{-}$  and  $\delta^2\text{H}\text{-CH}_4$  Source Signature Measurements, <https://doi.org/10.24416/UU01-YP43IN>, 2024.
- Oh, Y., Zhuang, Q., Welp, L. R., Liu, L., Lan, X., Basu, S., Dlugokencky, E. J., Bruhwiler, L., Miller, J. B., Michel, S. E., Schwietzke, S., Tans, P., Ciais, P., and Chanton, J. P.: Improved Global Wetland Carbon Isotopic Signatures Support Post-2006 Microbial Methane Emission Increase, *Communications Earth & Environment*, 3, 1–12, <https://doi.org/10.1038/s43247-022-00488-5>, 2022.
- 75 O'Rourke, P., Smith, S., Mott, A., Ahsan, H., McDuffie, E., Crippa, M., Klimont, Z., McDonald, B., Wang, S., Nicholson, M., Hoesly, R., and Feng, L.: CEDS V\_2021\_04\_21 Gridded Emissions Data, <https://doi.org/10.25584/PNNLDATAHUB/1779095>, 2021.

- Saunois, M., Stavert, A. R., Poulter, B., Bousquet, P., Canadell, J. G., Jackson, R. B., Raymond, P. A., Dlugokencky, E. J., Houweling, S., Patra, P. K., Ciais, P., Arora, V. K., Bastviken, D., Bergamaschi, P., Blake, D. R., Brailsford, G., Bruhwiler, L., Carlson, K. M., Carrol, M., Castaldi, S., Chandra, N., Crevoisier, C., Crill, P. M., Covey, K., Curry, C. L., Etiope, G., Frankenberg, C., Gedney, N., Hegglin, M. I., Höglund-Isaksson, L., Hugelius, G., Ishizawa, M., Ito, A., Janssens-Maenhout, G., Jensen, K. M., Joos, F., Kleinen, T., Krummel, P. B., Langenfelds, R. L., Laruelle, G. G., Liu, L., Machida, T., Maksyutov, S., McDonald, K. C., McNorton, J., Miller, P. A., Melton, J. R., Morino, I., Müller, J., Murguia-Flores, F., Naik, V., Niwa, Y., Noce, S., O'Doherty, S., Parker, R. J., Peng, C., Peng, S., Peters, G. P., Prigent, C., Prinn, R., Ramonet, M., Regnier, P., Riley, W. J., Rosentreter, J. A., Segers, A., Simpson, I. J., Shi, H., Smith, S. J., Steele, L. P., Thornton, B. F., Tian, H., Tohjima, Y., Tubiello, F. N., Tsuruta, A., Viovy, N., Voulgarakis, A., Weber, T. S., van Weele, M., van der Werf, G. R., Weiss, R. F., Worthy, D., Wunch, D., Yin, Y., Yoshida, Y., Zhang, W., Zhang, Z., Zhao, Y., Zheng, B., Zhu, Q., Zhu, Q., and Zhuang, Q.: The Global Methane Budget 2000–2017, *Earth System Science Data*, 12, 1561–1623, <https://doi.org/10.5194/essd-12-1561-2020>, 2020.
- Saunois, M., Martinez, A., Poulter, B., Zhang, Z., Raymond, P. A., Regnier, P., Canadell, J. G., Jackson, R. B., Patra, P. K., Bousquet, P., Ciais, P., Dlugokencky, E. J., Lan, X., Allen, G. H., Bastviken, D., Beerling, D. J., Belikov, D. A., Blake, D. R., Castaldi, S., Crippa, M., Deemer, B. R., Dennison, F., Etiope, G., Gedney, N., Höglund-Isaksson, L., Holgerson, M. A., Hopcroft, P. O., Hugelius, G., Ito, A., Jain, A. K., Janardanan, R., Johnson, M. S., Kleinen, T., Krummel, P. B., Lauerwald, R., Li, T., Liu, X., McDonald, K. C., Melton, J. R., Mühle, J., Müller, J., Murguia-Flores, F., Niwa, Y., Noce, S., Pan, S., Parker, R. J., Peng, C., Ramonet, M., Riley, W. J., Rocher-Ros, G., Rosentreter, J. A., Sasakawa, M., Segers, A., Smith, S. J., Stanley, E. H., Thanwerdas, J., Tian, H., Tsuruta, A., Tubiello, F. N., Weber, T. S., van der Werf, G. R., Worthy, D. E. J., Xi, Y., Yoshida, Y., Zhang, W., Zheng, B., Zhu, Q., Zhu, Q., and Zhuang, Q.: Global Methane Budget 2000–2020, *Earth System Science Data*, 17, 1873–1958, <https://doi.org/10.5194/essd-17-1873-2025>, 2025.
- Scarpelli, T. R., Jacob, D. J., Grossman, S., Lu, X., Qu, Z., Sulprizio, M. P., Zhang, Y., Reuland, F., Gordon, D., and Worden, J. R.: Updated Global Fuel Exploitation Inventory (GFEI) for Methane Emissions from the Oil, Gas, and Coal Sectors: Evaluation with Inversions of Atmospheric Methane Observations, *Atmospheric Chemistry and Physics*, 22, 3235–3249, <https://doi.org/10.5194/acp-22-3235-2022>, 2022.
- Stavert, A. R., Saunois, M., Canadell, J. G., Poulter, B., Jackson, R. B., Regnier, P., Lauerwald, R., Raymond, P. A., Allen, G. H., Patra, P. K., Bergamaschi, P., Bousquet, P., Chandra, N., Ciais, P., Gustafson, A., Ishizawa, M., Ito, A., Kleinen, T., Maksyutov, S., McNorton, J., Melton, J. R., Müller, J., Niwa, Y., Peng, S., Riley, W. J., Segers, A., Tian, H., Tsuruta, A., Yin, Y., Zhang, Z., Zheng, B., and Zhuang, Q.: Regional Trends and Drivers of the Global Methane Budget, *Global Change Biology*, 28, 182–200, <https://doi.org/10.1111/gcb.15901>, 2022.
- van Wees, D., van der Werf, G. R., Randerson, J. T., Rogers, B. M., Chen, Y., Veraverbeke, S., Giglio, L., and Morton, D. C.: Global Biomass Burning Fuel Consumption and Emissions at 500m Spatial Resolution Based on the Global Fire Emissions Database (GFED), *Geoscientific Model Development*, 15, 8411–8437, <https://doi.org/10.5194/gmd-15-8411-2022>, 2022.
- Weber, T., Wiseman, N. A., and Kock, A.: Global Ocean Methane Emissions Dominated by Shallow Coastal Waters, *Nature Communications*, 10, 4584, <https://doi.org/10.1038/s41467-019-12541-7>, 2019.